waste

MDPI

Article

Phytomining: Powering the Circular Future of Silver Extraction

Darragh Doyle [1,*], Federico Trotta [2], Danielle Winning [2], Uche Onwukwe [3,4] and Lorna Anguilano [3,4,*]

[1] Department of Chemical Engineering, Brunel University of London, London UB8 3PH, UK
[2] Metalchemy Limited, London WC2H 9JQ, UK; ft@metalchemy.tech (F.T.); dw@metalchemy.tech (D.W.)
[3] Experimental Techniques Centre, Brunel University of London, London UB8 3PH, UK; uche.onwukwe@brunel.ac.uk or uche@phyona.co.uk
[4] Phyona Limited, Lincolnshire PE9 2PF, UK
* Correspondence: darragh.doyle@brunel.ac.uk (D.D.); lorna.anguilano@brunel.ac.uk or lorna@phyona.co.uk (L.A.)

Abstract

Phytomining offers a sustainable and environmentally benign strategy for recovering valuable metals from contaminated or low-grade substrates. In this study, *Agrostis capillaris*, *Mentha spicata*, and *Lavandula angustifolia* were assessed for their phytomining potential when exposed to silver nitrate and a commercial silver-containing waste stream. Quantitative X-ray fluorescence (XRF) analysis revealed species-specific differences in silver uptake and translocation; *L. angustifolia* exhibited the highest tissue silver concentrations under both treatments, reaching 5980 parts per million (ppm) following silver nitrate exposure and 91 ppm following commercial waste exposure. These higher tissue concentrations may partly reflect differences in plant biomass and species-specific uptake or retention characteristics. In contrast, *A. capillaris* exhibited the highest bioaccumulation factor (BAF) with a value of 2.15 under nitrate treatment and 0.78 under commercial waste exposure, indicating comparatively greater accumulation relative to the corresponding substrate conditions. Ultramicrotomy and scanning electron microscopy with energy-dispersive X-ray spectroscopy and backscattered electron (SEM-EDS-BSE) imaging confirmed the in vivo biosynthesis of silver nanoparticles (Ag-NPs), with distinct morphologies and spot analyses of silver weight percentages (Wt%) ranging from 16.7–72.6 Wt%. These findings underscore the dual capacity of selected herbaceous plants to extract bioavailable ionic silver and mediate the intracellular formation of Ag-NPs. The integration of XRF and SEM-EDS-BSE techniques provides a robust framework for evaluating phytomining systems, highlighting the potential of these species as biorefineries for noble metal nanoparticle recovery. Such approaches align with emerging circular economy principles and bio-nanotechnology development.

Keywords: phytomining; silver nanoparticles; colloidal silver; bioaccumulation; biotechnology; waste

Check for updates

Academic Editor: Christopher Cheeseman

Received: 21 October 2026
Revised: 30 October 2026
Accepted: 5 November 2026
Published: 10 November 2026

Copyright: © 2026 by the authors. Licensee MDPI, Basel, Switzerland. This article is an open access article distributed under the terms and conditions of the Creative Commons Attribution (CC BY) license.

1. Introduction

Phytomining refers to the use of hyperaccumulator plants to extract valuable metals from soil or industrial waste through biological uptake mechanisms. Unlike conventional mining supplements, phytomining operates with minimal environmental disruption and lower energy input, offering a promising strategy for additional metal recovery from marginal or polluted lands. With global demand exceeding 30,000 metric tonnes annually and growing due to its applications in electronics, catalysis, healthcare, and food packaging, sustainable recovery pathways have become increasingly important [1]. In 2024, the market for silver nanoparticles (Ag-NPs) was valued at 4 billion USD, with projections reaching

12.1 billion USD by 2034 at a compound annual growth rate (CAGR) of 11.7% (2025–2034). Likewise, the broader colloidal silver (CS) market reached 1.4 billion USD in 2024 and is forecast to grow to 3.4 billion USD by 2035, following a CAGR of 8.18% (2025–2035). In both markets, North America represents the largest regional share (Ag-NPs in 2023; CS in 2024) [2]. Among various target elements, Silver (*Ag*) has gained industrial significance and toxicological footprint within ecosystems when improperly managed. Recent advancements in bio-nanotechnology have further expanded the scope of phytomining by demonstrating the ability of plants to biosynthesise metal nanoparticles [3]. Plant tissues serve not only as bioaccumulators but also as reducing and capping agents for nanoparticle formation, particularly in the case of noble metals such as silver. This biogenic synthesis is driven by phytochemicals, including phenolics, flavonoids, and terpenoids, which reduce metal ions and stabilise nanoparticles within plant tissues [4]. While several species have been explored for their Ag-NP biosynthesis capability, herbaceous plants such as *Agrostis capillaris*, *Mentha spicata*, and *Lavandula angustifolia* remain underexplored for their dual phytoremediation and nanomaterial production potential. The integration of analytical techniques such as XRF for elemental analysis and SEM-EDS-BSE for nanoparticle imaging enhances the understanding of nanoparticle accumulation and formation. This study aims to assess these species' performance under controlled silver exposure conditions and evaluate their suitability for phytomining applications in bio-nanotechnology and resource recovery frameworks [5].

The bioaccumulation factor (BAF) is a widely employed index in phytomining and phytotechnology, implemented to quantify the ability of plants to accumulate noble metals or other contaminants from their growing medium. It is defined as the ratio of the concentration of a specific element in plant tissues to its corresponding concentration within soil, on a dry weight (DW) basis [6]. The BAF (Equation (1)) is expressed as:

$$\text{Bioaccumulation Factor (BAF)} = \frac{\text{Concentration}_{\text{Tissue}}}{\text{Concentration}_{\text{Soil}}}, \quad (1)$$

where C_{Tissue} represents the concentration of noble metals in the plant tissue (mg kg^{-1} DW), and C_{Soil} denotes the concentration of the same elements in the substrate (mg kg^{-1} DW). A BAF value greater than 1 indicates that the plant tissue accumulates the element to a concentration exceeding its availability within the soil, a desirable trait characteristic of hyperaccumulator species [7].

In phytomining applications, BAF serves not only as a metric for accumulation but also as a critical screening parameter for identifying candidate species capable of extracting economically or environmentally significant elements. Species exhibiting BAF values substantially greater than unity are considered more effective for phytomining strategies. Conversely, species with BAF ≤ 1 are often excluded from such applications due to limited uptake efficiency [8].

The utility of BAF extends to the risk assessment of agroecological contexts, where elevated values for toxic metals in edible crops can signal potential health risks to consumers. In such cases, the index helps delineate safe cultivation zones and guides remediation efforts via phytomining. Several studies have employed BAF to assess the accumulation potential of various crops under metal-stressed conditions, providing insights into soil–plant transfer dynamics and pathways [9].

More recently, the concept of bioaccumulation has been extended to the uptake of nanomaterials, including noble metals such as silver (*Ag*). These materials, due to their increasing use in industrial and medical applications, are emerging as environmental contaminants. In the context of phytomining of nanoparticles, BAF is recalibrated to quantify the accumulation of nanoparticulate material within plant tissues relative to their concentrations within the substrate, despite the inherent challenges in speciation and quantification. The uptake,

translocation, and morphology of silver nanoparticles (Ag-NPs) within plants are complex processes, influenced by aspects such as particle size, nucleation, and mineralogy [10].

Given the analytical complexities associated with characterising *Ag* uptake and transformation, the application of BAF requires integration of advanced analytical techniques. X-ray fluorescence (XRF) provides non-destructive, quantitative elemental analysis across plant tissue, enabling knowledge of metal distribution. X-ray diffraction (XRD) identifies the crystalline structures of accumulated nanoparticles, determining tactility and phase transformation. Scanning electron microscopy (SEM) combined with energy-dispersive spectroscopy (EDS) and backscattered electron (BSE) imaging allows high-resolution imaging and elemental composition analysis at the micro and nanoscale, enabling the detection and localisation of metal nanoparticles across phytomining processes, thereby refining the interpretation of BAF in environmental and phytomining studies.

Several studies have reported successful internalisation of Ag-NPs in terrestrial plant species, with indications of accumulation in roots and limited translocation and compartmentalisation to aerial tissues (above ground). For example, experiments involving *Brassica juncea* and *Lemna minor* (aquatic species) have demonstrated BAF values exceeding unity under controlled exposure conditions, suggesting that such species may serve as potential agents for phytomining of nanoparticles [11].

Plants have demonstrated potential in the mediation and production of nanoparticles in comparison to conventional methods. Advantages include potential environmental friendliness, cost-effectiveness, and scalability due to the prominence of contaminated soil and low-grade ores. In phytomining synthesis of nanoparticles, plant tissues facilitate the conversion of metallic ions into stable nanoparticles. This process is driven by a range of phytochemicals such as flavonoids, phenolics, and terpenoids, which actively participate in the nucleation and stabilisation of fine silver particulates. The green synthesis approach via phytomining has gained promise due to its compatibility with sustainable technology, especially in the context of noble metals such as silver (*Ag*) [12].

Over the past decade, numerous species have been investigated for their ability to accumulate and synthesise Ag-NPs, with some identified as potential hyperaccumulators. These species exhibit not only efficient uptake of *Ag* ions but also internal stabilisation of Ag-NPs within their tissues. Table 1 displays the findings of recent projects involving several plant species used in the production of Ag-NPs. The growing interest in Ag-NPs stems from their wide-ranging applications in antimicrobial coatings, drug delivery systems, food packaging, biosensors, and diagnostic platforms, making phytomining a compelling supplement to nanomaterial production [13].

Table 1. Reported herbaceous plant species used for silver (*Ag*) accumulation and nanoparticle formation, including nanoparticle size and predominant plant tissue compartment [13].

Species	Compartmentalisation	Nanoparticulate Size (nm)
Chenopodium murale	Foliage	30–50 nm
Cissus quadrangularis	Foliage	15–23 nm
Stevia rebaudiana	Foliage	2–50 nm
Origanum vulgare	Foliage	10–140 nm
Capsicum annuum	Foliage	5–60 nm
Coccinia grandis	Foliage	20–30 nm
Catharanthus roseus	Foliage	27–32 nm
Rosa damascena	Foliage	10–30 nm

Several herbaceous plant species have demonstrated the ability to accumulate, translocate, and compartmentalise *Ag* into nanoparticles, highlighting their potential for phytomining applications. As shown in Table 1, all eight species localise Ag-NPs predominantly

within their foliage, indicating efficient uptake and compartmentalisation in above-ground tissues. *S. rebaudiana* exhibited the widest nanoparticle size range (2–50 nm), while *C. murale* produced the smallest, more uniform particles (7–15 nm, suggesting species-specific reduction capabilities. *O. vulgare* generated the largest Ag-NPs (10–140 nm), reflecting variable phytochemical influences on nanoparticle morphology.

2. Materials and Methods

2.1. Species Selection

A targeted range of accumulators and fast-growing biomass species were selected for noble metal phytomining trials. These include *Agrostis capillaris*, *Mentha spicata*, and *Lavandula angustifolia*. Selection criteria were based on root architecture, biomass yield, known capabilities, and compatibility with post-harvesting.

2.2. Doping Regime and Growth Monitoring

Species were cultivated in two separate controlled organic (John Innes No.2 Topsoil, Norwich, UK) substrate conditions, doped with (Total = 0.1 M/1L-1 Month) Silver (*Ag*) nitrate salts (Fisher Scientific, PA, USA) and (Total = 1.75 L of liquid waste, diluted in 1.55 L of mains water) colloidal silver (CS) commercial waste (Metalchemy Ltd., London, UK). Prior to dosing, the CS commercial waste was characterised for *Ag* content, with X-ray fluorescence (Rigaku NEX DE XRF, Rigaku, Tokyo, Japan) indicating 212 ppm *Ag* concentration and trace *Al*, *Si*, and *Ca*. Scanning electron microscopy (Tescan Magna GMU SEM, TESCAN, Brno, Czech Republic) with backscattered electrons (BSE) and energy-dispersive X-ray spectroscopy (EDS) spot analysis further identified 37.7 Wt% *Ag*, confirming the presence of concentrated *Ag*-bearing particulates in the CS waste. *A. capillaris*, *M. spicata*, and *L. angustifolia* were individually dosed via aqueous solutions to assess their phytomining potential. Growth tracking was conducted over two key intervals: initially, following planting and plant stabilisation, to establish baseline development, and subsequently prior to harvest, after a one-month accumulation period. This approach enabled evaluation of the species' tolerance to *Ag* exposure and capacity to uptake over time.

2.3. Sample Collection and Pruning

Above-ground biomass was periodically pruned and collected. Samples were oven-dried (65 °C-24 h) and prepared for X-Ray Diffraction (Rigaku SuperNova XRD, Rigaku, Tokyo, Japan) and XRF to determine *Ag* mineralogical phase states, accumulation within the plant tissue, and the bioaccumulation factors (BAF; Equation (1)).

2.4. Ultramicrotome Cross-Sectioning

The selected samples underwent ultrastructural embedding in a four-part low-viscosity resin system composed of resin, hardener, low-viscosity hardener, and accelerator (Agar Scientific, Sheffield, UK). Following curing, ultrathin sections were cut via ultramicrotomy (PowerTome PC CR-X, Boeckeler Instruments, Tucson, AZ, USA) using glass knives. Sections were mounted on glass slides and carbon-coated (Agar Turbo Carbon Coater, Agar Scientific, Sheffield, UK) for SEM (Gemini Supra 35VP SEM, ZEISS, Oberkochen, Germany) analysis with EDS/BSE. This provided insight into intracellular *Ag* distribution and compartmentalisation within plant tissues.

2.5. Biomass Harvesting and Aerobic Bioextraction Process

Upon confirming adequate *Ag* uptake, translocation, and compartmentalisation, full biomass of target species was harvested. Samples were stored under specific conditions to prevent contamination of nanoparticulate-rich material. Plant biomass enriched with

Ag underwent biodigestion using a commercial (Phyona Ltd., Lincolnshire, UK) low toxicity/energy system optimised for *Ag* liberation while preserving nanoparticulate integrity. Controlled thermal cycling supported the breakdown of plant matrices and exposure of metal particles.

2.6. Liquid Residue Filtration

Post-extraction mixtures were stirred and filtered sequentially through three pore-size filters: qualitative paper, 16 µm, and 2.5 µm membranes. This stratified Ag-NPs based on agglomeration and size distribution, capturing a spectrum of nanoparticulate forms from loosely bound clusters to finer crystalline particles.

2.7. SEM Analysis of Filtrates

Aliquots from each filtration fraction were oven-dried (45 °C-30 min), carbon-coated, and analysed using SEM-EDS/BSE to evaluate elemental composition, distribution, particle size, and capture efficiency of each filter grade. This stage offered insights into particle morphology and aggregation behaviour during extraction.

2.8. Filtration Residue Recovery

Captured Ag-NPs were retrieved from filter media using ultrasonication (Solbraze Ltd., Shipley, UK) combined with low-heat stirring to dislodge particles. Resulting suspensions were centrifuged (Heraeus Labfuge 400R, Heraeus, Hessen, Germany) to concentrate Ag-NPs. Collected samples were deposited on silicon wafers, carbon-coated, and examined via SEM-EDS/BSE for morphological integrity and compositional fidelity post-extraction and recovery.

3. Results and Discussion

3.1. Silver Uptake and Bioaccumulation from Nitrate Salt Treatment

X-Ray Fluorescence (XRF) quantification revealed distinct uptake capabilities of *Agrostis capillaris*, *Mentha spicata*, and *Lavandula angustifolia* in response to silver nitrate exposure (Table 2). Among the three species, *L. angustifolia* demonstrated the highest *Ag* tissue concentration (5980 ppm), followed by *M. spicata* (3860 ppm) and *A. capillaris* (795 ppm).

Table 2. Tissue *silver* (*Ag*) concentrations and bioaccumulation factor (BAF) for *A. capillaris*, *M. spicata*, and *L. angustifolia* following *silver* nitrate treatment (ppm).

Species (Tissue Concentration)	**Noble Metal (Nitrate Salt) (Parts Per Million, PPM)**	
	Ag	
		BAF
Agrostis capillaris	795	2.15
Mentha spicata	3860	1.49
Lavandula angustifolia	5980	0.64

However, when normalised alongside the corresponding substrate (soil) concentrations (Table 3), *A. capillaris* exhibited the highest bioaccumulation factor (BAF) of 2.15, suggesting superior root-to-shoot regional zone translocation efficiency under nitrate-derived *Ag* input. Conversely, *L. angustifolia* displayed a lower BAF (0.64), likely due to its high soil concentration (9280 ppm), indicating limited translocation or high rhizosphere retention.

Table 3. Substrate (soil) *silver* (*Ag*) concentrations associated with *A. capillaris*, *M. spicata*, and *L. angustifolia* following *silver* nitrate treatment (ppm).

Species (Soil Concentration)	**Noble Metal (Nitrate Salt) (Parts Per Million, PPM)**
	Ag
Agrostis capillaris	370
Mentha spicata	2590
Lavandula angustifolia	9280

These findings are consistent with previous studies indicating species-specific variations in metal ion accumulation, which may stem from physiological traits such as radix structure or compound profiles. The enhanced uptake in *M. spicata* and *L. angustifolia* could also be attributed to secondary metabolites which act as natural reducing agents, not only facilitating ion uptake, but also particle bioreduction within foliar tissues.

3.2. Silver Uptake from Commercial Waste

In the second treatment set involving an *Ag*-containing commercial waste stream (Metalchemy Ltd.), all species demonstrated markedly lower accumulation (Table 4). Tissue concentrations of *Ag* dropped significantly compared to the nitrate treatment, with *A. capillaris* accumulating 14 ppm, *M. spicata* 24 ppm, and *L. angustifolia* 91 ppm.

Table 4. Tissue *silver* (*Ag*) concentrations and bioaccumulation factor (BAF) for *A. capillaris*, *M. spicata*, and *L. angustifolia* following exposure to the *silver*-containing commercial waste stream (ppm).

Species (Tissue Concentration)	**Noble Metal (Commercial Waste-Colloidal Silver) (Parts Per Million PPM)**	
	Ag	
		BAF
Agrostis capillaris	14	0.78
Mentha spicata	24	0.08
Lavandula angustifolia	91	0.16

Substrate *Ag* levels (Table 5) ranged from 18 ppm to 570 ppm, resulting in lower BAF values across all species. Notably, *A. capillaris* again showed the highest BAF (0.78), further highlighting its relative efficiency under complex matrix conditions.

Table 5. Substrate (soil) *silver* (*Ag*) concentrations associated with *A. capillaris*, *M. spicata*, and *L. angustifolia* following exposure to the *silver*-containing commercial waste stream (ppm).

Species (Soil Concentration)	**Noble Metal (Commercial Waste-Colloidal Silver) (Parts Per Million PPM)**
	Ag
Agrostis capillaris	18
Mentha spicata	311
Lavandula angustifolia	570

3.3. SEM-EDS Characterisation of Biogenic Silver Particles

SEM-EDS analysis confirmed the formation of biogenic Ag-NPs in all three species across both treatment conditions post-qualitative filtration (Figure 1). In *A. capillaris*, Ag-NPs formed under nitrate exposure (Figure 1A) displayed densely aggregated morphologies with uniform particle distribution across a large calcium (*Ca*) rich crystal, with a localised *Ag* signal of up to 63 Wt% *Ag*. In contrast, under the commercial waste stream treatment (Figure 1B), aggregation was still evident, though less uniform, and the measured *Ag* content decreased to 48 Wt%. This reduction does not necessarily indicate a lower silver Wt% content within the *Ag*-containing nanoparticulate but rather reflects a broader EDS beam interaction with surrounding substrate material. Less dense clustering of Ag-NPs and increased presence of background elements influenced output.

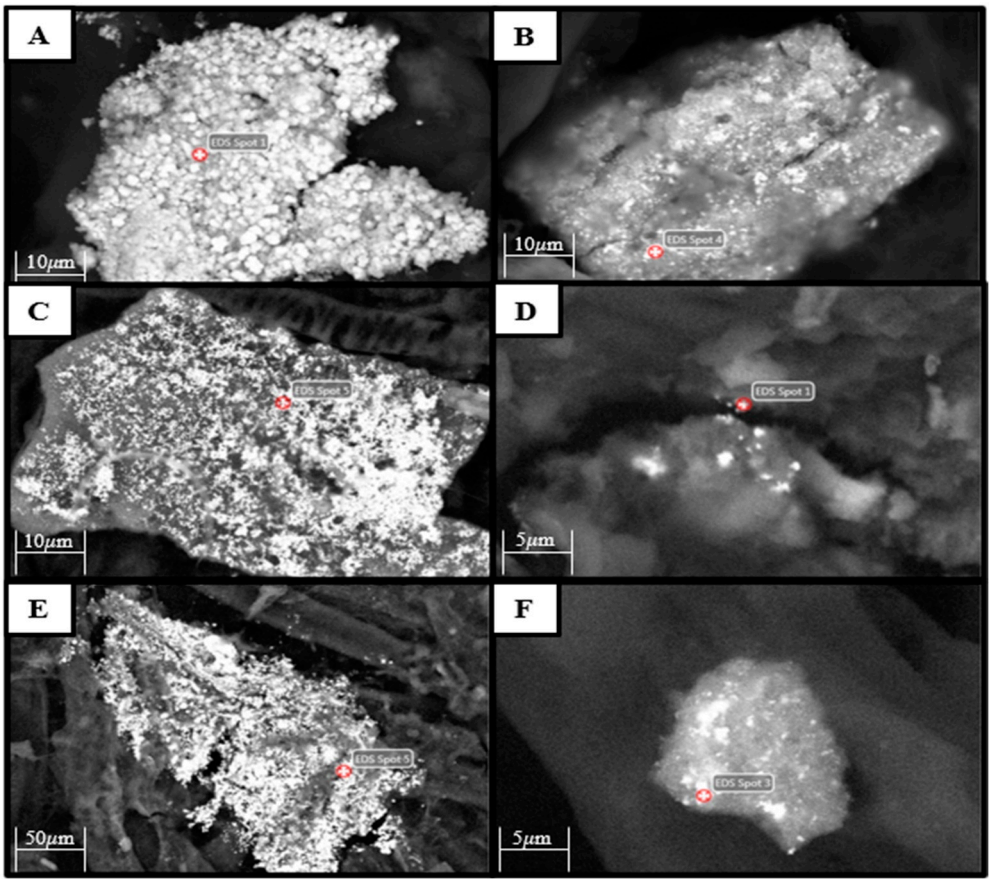


Figure 1. SEM-EDS Characterisation of *silver* nanoparticles recovered from *A. capillaris* (**A**,**B**), *M. spicata* (**C**,**D**), and *L. angustifolia* (**E**,**F**) following qualitative filtration. Panels (**A**,**C**,**E**) show the *silver*-nitrate treatment; panels (**B**,**D**,**F**) show the commercial waste treatment.

In *M. spicata*, nitrate-derived particles (Figure 1C) showed widespread nanoscale deposition with an associated *Ag* signal of 34 Wt%, whereas the commercial waste treatment (Figure 1D) produced smaller, isolated particles with a comparable, higher *Ag* signal of 47 Wt%, likely due to reduced substrate interference. *L. angustifolia* produced extensive nanoparticulate coverage under nitrate conditions of 51 Wt% (Figure 1E), while the waste-derived silver nanoparticle recovery was sparser and morphologically less crystalline in appearance, registering at 22 Wt% *Ag* (Figure 1F). Across all samples, minor co-localised elements such as *Cl*, *Ca*, and *P* were observed, primarily from the remnant organic plant matrix or mineral substrate.

3.4. Morphological Differentiation of Extracted Silver Particles via Ultrasonic Liberation

SEM-EDS/BSE analysis of filtrates collected after ultrasonication and centrifugation revealed clear morphological and compositional trends across species and treatment types (Figure 2). These datasets reflect not only the differences in nanoparticle biosynthesis pathways among *A. capillaris*, *M. spicata*, and *L. angustifolia*, but also the influence of ionic versus colloidal silver sources on nanomaterial aggregation, mineral identification, and association with organic matrices.

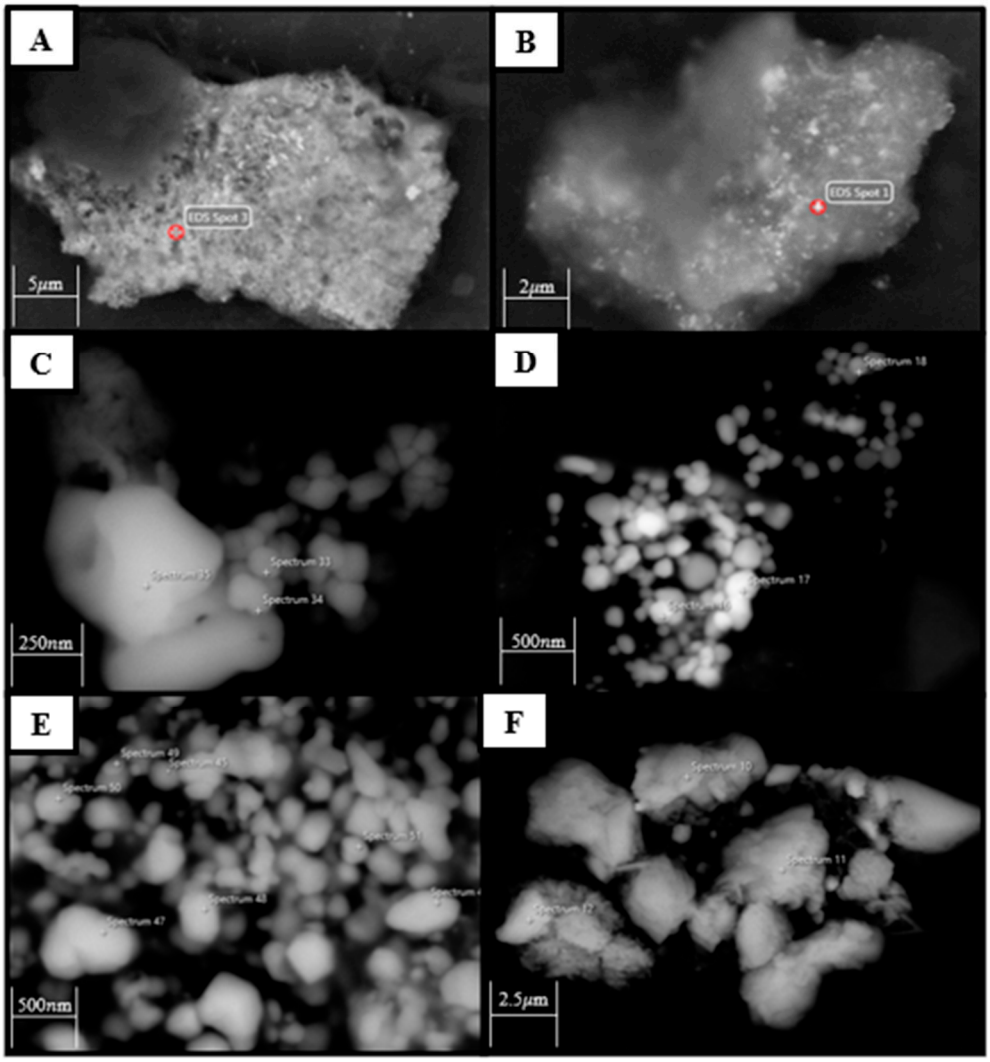


Figure 2. Morphology and elemental composition of *silver*-bearing particles liberated by ultrasonication from *A. capillaris* (**A**,**B**), *M. spicata* (**C**,**D**) and *L. angustifolia* (**E**,**F**), characterised by SEM-EDS-BSE. For each species, the first panel represents *silver*-nitrate exposure, and the second panel represents commercial-waste exposure.

3.4.1. *Agrostis capillaris*

Under nitrate salt exposure, *A. capillaris* produced distinct *Ag*-bearing nanominerals following dislodgement (Figure 2A). Particles appeared as compact clusters decorating a *Ca*/*Cl*-rich substrate. EDS spot analyses showed ~54.52 Wt% *Ag*. In contrast, the commercial waste treatment (Figure 2B) yielded smaller, loosely bound colloidal particles with a lower *Ag* signal (29.75 Wt%). The difference in Wt% is consistent with increased beam interaction with surrounding *Ca*-*Cl*-dominated mineral substrate in the loosely packed agglomerates rather than reflecting actual differences in *Ag* purity, suggesting that *A. capillaris* forms

denser *Ag* coatings when the precursor is fully ionic, whereas colloidal waste inputs produce weaker nucleation and more heterogeneous particulate attachment.

3.4.2. *Mentha spicata*

Nitrate-derived Ag-NPs from *M. spicata* formed large submicron *Ag*-rich clusters (~32.1 Wt%), exhibiting smooth surfaces with early-stage nucleation (Figure 2C). Conversely, exposure to commercial waste resulted in highly defined, crystalline colloidal silver aggregates (~59.3 Wt%), indicating enhanced liberation of *Ag* from the plant matrix following ultrasonication (Figure 2D). These particles were significantly smaller, more numerous, and more spatially discrete than in the nitrate condition. The higher apparent *Ag* Wt% in the waste-derived sample is attributable to reduced interference from the organic residue and fewer adjacent mineralogical phases, resulting in more *Ag*-dominant interaction volumes during EDS acquisition.

3.4.3. *Lavandula angustifolia*

L. angustifolia formed dense, highly polydisperse Ag-NP populations (Figure 2E) with clear nanoparticulate organisation (54.5 Wt%) under nitrate exposure. The structures suggest nucleation facilitated by phytochemicals abundant in aromatic herbaceous species such as *L. angustifolia* and *M. spicata*, such as terpenoids and phenolic acids. Commercial waste-derived particles (Figure 2F) appeared as larger colloidal mineral aggregates (~72.6 Wt%), but with lower morphological uniformity. Their high apparent Wt% again reflects reduced beam overlap with organic matrices, not differences in metallic purity. The larger particle size ~2.5 µm indicates aggregation post-biosynthesis, likely during filtration or release.

3.5. Intracellular Localisation of Ag-NPs in Epidermal Tissues

Ultramicrotome cross-sections revealed compelling evidence of intracellular *Ag* compartmentalisation within the upper epidermis of all three species following nitrate exposure (Figure 3). The clear localisation of *Ag*-bearing particles within defined cellular regions strongly supports the occurrence of in vivo mineralisation, rather than additional artifacts associated with extraction, filtration, or liberation. These observations align with proposed phytochemical-driven reduction pathways in higher plants, where ions are transported, complexed, and subsequently reduced within specialised cellular microenvironments.

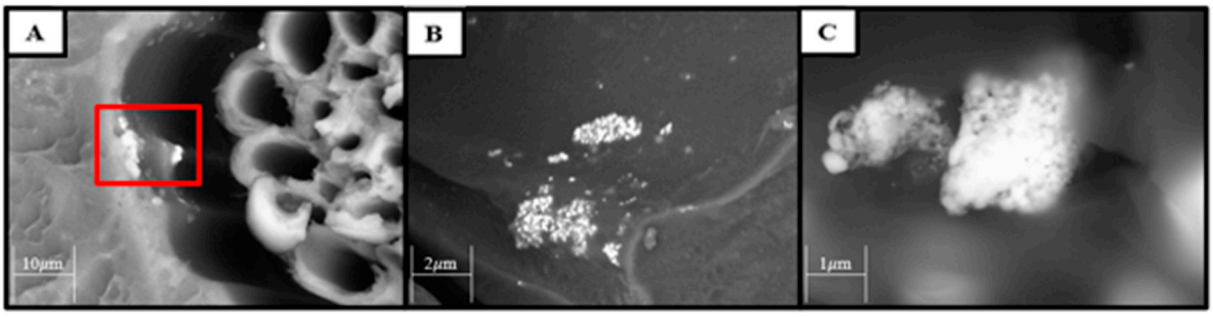


Figure 3. Intracellular distribution and compartmentalisation of *silver*-bearing nanoparticles within the upper epidermal tissues of *A. capillaris* (**A**), *M. spicata* (**B**), and *L. angustifolia* (**C**) revealed by ultramicrotome cross-sections and SEM-EDS-BSE analysis.

3.5.1. *Agrostis capillaris*

A. capillaris shows a well-defined *Ag* nanomineral (16.7 Wt%) embedded within the epidermal tissue (Figure 3A). The particles appear to sit within a discrete cellular cavity, suggesting that nucleation occurred internally rather than through surface adsorption or

extracellular deposition. The adjacent tissue contains *Ca* and *Cl* elements typical of cell wall and middle lamella regions, supporting the interpretation that *Ag* is incorporated during intracellular transport rather than passively deposited.

3.5.2. *Mentha spicata*

M. spicata displayed concentrated *Ag* nanoparticle clusters (~26.6 Wt%) distributed along internal cell wall surfaces (Figure 3B), indicating a more extensive interaction between *Ag* species and structural polysaccharides. The distribution pattern suggests active intracellular transport mechanisms, potentially involving metal-binding peptides, membrane transporters, or vacuolar sequestration pathways. Such localisation is consistent with known detoxification responses in aromatic herbaceous species, where secondary metabolites can help stabilise reduced nanoparticles.

3.5.3. *Lavandula angustifolia*

In *L. angustifolia*, compact *Ag*-rich aggregates (22.8 Wt%) were observed within enclosed epidermal compartments (Figure 3C). Their crystalline appearance and well-defined boundaries suggest efficient in situ reduction of *Ag*, likely mediated by *L. angustifolia* high concentrations of terpenoids, phenolics, and antioxidant compounds. These phytochemicals are recognised for their strong reducing capacity and ability to stabilise metal nanoparticles, which may explain the more structured mineral forms observed in the species.

3.6. Study Duration, Environmental Exposure and Future Experimental Design

The one-month accumulation period used in this study provided a defined and practical interval for comparing short-term silver uptake, tissue distribution and nanoparticle formation across the three plant species. However, this duration also limits the ecological and biological conclusions that can be drawn. A single short-term exposure cannot establish whether the observed uptake patterns persist during longer growth, whether silver causes delayed or cumulative phytotoxic effects, or whether reproductive endpoints are affected. In particular, the present design did not assess flowering, seed production, seed viability, germination, seedling vigor, or the possible transfer of silver to seeds. It therefore cannot determine reproductive toxicity or heritable effects across successive plant generations. Nor can it fully capture seasonal changes in biomass production, root development, plant health, or the stability and remobilisation of silver within aging tissues.

Longer experiments would also allow time-dependent transformations of silver in the substrate and rhizosphere to be investigated. For example, sulphidation can convert bioavailable silver species into sparingly soluble silver sulphide, generally reducing silver mobility and changing its bioavailability. Such transformations may require longer exposure and aging periods than those examined here. Prolonged trials could therefore distinguish initial uptake from subsequent immobilisation, remobilisation and changes in silver speciation, while also revealing whether nanoparticle morphology and intracellular localisation remain stable over time. These processes are important when interpreting plant uptake under environmentally realistic conditions.

Accordingly, future work should extend exposure across multiple growth stages and, where feasible, complete reproductive cycles and successive generations. A time series design should combine measurements of plant growth and biomass, root and stem silver concentrations, silver speciation in soil and plant tissues, nanoparticle characteristics, flowering and seed traits, and post-harvest recovery yields. Experiments using aged substrates and environmentally relevant inputs, including realistic concentrations, repeated or intermittent loading, and relevant soil chemistry, would more closely reproduce ecological exposure

sequences than a single one-month dosing period. These longer-term studies are needed to assess both the persistence of phytomining performance and potential ecological risks.

4. Conclusions

The results show that the selected plant species can accumulate and compartmentalise silver from different sources and can mediate the formation of silver-bearing nanoparticles. This supports further investigation of plant-based systems as components of bio-nanotechnology and resource recovery strategies, particularly for the remediation and valorisation of silver-containing waste streams. Modern phytomining should be viewed not simply as metal removal by plants, but as an integrated, circular process linking the treatment of low-grade ores or secondary waste resources with biomass production, controlled harvesting, metal recovery and potential reuse of recovered materials. Its longer-term value will depend on demonstrating reliable metal yields, selectivity, economic viability, safe management of contaminated biomass and limited ecological impacts under realistic operating conditions. The present findings provide proof-of-concept evidence for silver uptake and biogenic particle formation, but do not yet establish commercial-scale productivity or environmental safety.

The combined XRF, microtomy cross-sections, and SEM-EDS-BSE results affirm the viability of *Agrostis capillaris*, *Mentha spicata*, and *Lavandula angustifolia* as silver nanoparticle phytomining candidates, with *A. capillaris* emerging as the most promising under both ionic and industrially complex conditions. Although overall uptake from the commercial waste was comparatively lower, successful particle formation across all species indicates that phytomining could be adapted to handle industrial byproducts with effective pretreatment strategies or soil amendments. Furthermore, the morphological data from SEM-EDS-BSE suggest that silver particles/colloidal silver formed in vivo may be directly harvestable for downstream applications, minimalising the need for further processing.

Importantly, the mechanisms demonstrated here may also be applicable to the extraction and particle biosynthesis of high-value or critical metals, including *Au*, *Pt*, and *Cu*, particularly in low-grade or waste-derived matrices supplied by commercial waste streams (Metalchemy Ltd.).

In conclusion, plant species can not only uptake and compartmentalise silver from diverse sources but also synthesise Ag-NPs with tuneable characteristics. This supports their use in bio-nanotechnology and resource recovery strategies, particularly in systems designed for the sustainable remediation of silver-laden waste streams.

Author Contributions: D.D.: Conceptualisation, data curation, formal analysis, investigation, methodology, resources, software, validation, visualisation, writing—original draft, review and editing. F.T.: Conceptualisation, funding acquisition, resources, validation, visualisation, writing—review and editing. D.W.: Conceptualisation; resources, validation, visualisation, writing—review and editing. U.O.: Conceptualisation, investigation, methodology, project administration, resources, software, supervision, validation, visualisation, writing—review and editing. L.A.: Conceptualisation, funding acquisition, investigation, methodology, project administration, resources, software, supervision, validation, visualisation, writing—review and editing. All authors have read and agreed to the published version of the manuscript.

Funding: This project has received funding from the EPSRC, Place Based Impact Acceleration Account Programme Grant No: EP/Y023846/1—Park Royal PBIAA Net-Zero Food Supply Chains.

Data Availability Statement: The original contributions presented in this study are included in the article. Further inquiries can be directed to the corresponding author.

Acknowledgments: The authors gratefully acknowledge the support of Brunel University of London and the Experimental Techniques Centre (ETC) for providing access to advanced analytical instru-

mentation and technical expertise critical to this study. We also extend our sincere thanks to Phyona Limited and Metalchemy Limited for their contribution of specialist materials and nanotechnology insights, which greatly enriched the scope of this work. The collaboration and resources provided by these institutions were instrumental in the successful execution of this research.

Conflicts of Interest: Authors Federico Trotta and Danielle Winning were employed by Metalchemy Limited, London, UK. Authors Uche Onwukwe and Lorna Anguilano were employed by Phyona Limited, Lincolnshire, UK. The remaining author declares that the research was conducted in the absence of any commercial or financial relationships that could be construed as a potential conflict of interest.

Abbreviations

The following abbreviations are used in this manuscript:

XRF	X-Ray Fluorescence
SEM	Scanning Electron Microscopy
EDS	Energy Dispersive Spectroscopy
BSE	Backscattered Electrons
Ag-NPs	Silver Nanoparticles
USD	United States Dollar
CS	Colloidal Silver
BAF	Bioaccumulation Factor
DW	Dry Weight
XRD	X-Ray Diffraction
L	Litre
Hrs	Hours
°C	Degree Celsius
Mins	Minutes
ppm	Parts Per Million
Wt%	Weight Percent
µm	Micrometre
Ltd	Limited

References

1. Chaney, R.L.; Angle, J.S.; Broadhurst, C.L.; Peters, C.A.; Tappero, R.V.; Sparks, D.L. Improved Understanding of Hyperaccumulation Yields Commercial Phytoextraction and Phytomining Technologies. *J. Environ. Qual.* **2007**, *36*, 1429–1443. [CrossRef] [PubMed]
2. Karn, R.; Mawlankar, N.; Prasad, E. Allied Market Research. May 2025. Available online: https://www.alliedmarketresearch.com/silver-nanoparticles-market-A06923 (accessed on 5 December 2025).
3. Iravani, S. Green synthesis of metal nanoparticles using plants. *Green Chem.* **2011**, *13*, 2638–2650. [CrossRef]
4. Ahmed, S.; Saifullah; Ahmad, M.; Swami, L.B.; Ikram, S. Green synthesis of silver nanoparticles using *Azadirachta indica* aqueous leaf extract. *J. Radiat. Res. Appl. Sci.* **2016**, *9*, 1–7. [CrossRef]
5. Ali, H.; Khan, E.; Sajad, M.A. Phytoremediation of heavy metals—Concepts and applications. *Chemosphere* **2013**, *91*, 869–881. [CrossRef] [PubMed]
6. Yoon, J.; Cao, X.; Zhou, Q.; Ma, L.Q. Accumulation of Pb, Cu, and Zn in native plants growing on a contaminated Florida site. *Sci. Total Environ.* **2006**, *368*, 456–464. [CrossRef] [PubMed]
7. Reeves, R.D.; Baker, A.J.M. *Metal-Accumulating Plants. Phytoremediation of Toxic Metals: Using Plants to Clean Up the Environment*; John Wiley and Sons, Inc.: New York, NY, USA, 2000.
8. Wang, G.; Su, M.-Y.; Chen, Y.-H.; Lin, F.-F.; Luo, D.; Gao, S.-F. Transfer Characteristics of Cadmium and Lead from Soil to the Edible Parts of Six Vegetable Species in Southeastern China. *Environ. Pollut.* **2006**, *144*, 127–135. [CrossRef] [PubMed]
9. Ma, X.; Geiser-Lee, J.; Deng, Y.; Kolmakov, A. Interactions between engineered nanoparticles (ENPs) and plants: Phytotoxicity, uptake and accumulation. *Sci. Total Environ.* **2010**, *408*, 3053–3061. Corrigendum in *Sci. Total Environ.* **2014**, *481*, 635. [CrossRef] [PubMed]
10. Schwab, F.; Zhai, G.; Kern, M.; Turner, A.; Schnoor, J.L.; Wiesner, M.R. Barriers, pathways and processes for uptake, translocation and accumulation of nanomaterials in plants—Critical review. *Nanotoxicology* **2015**, *10*, 257–278. [CrossRef] [PubMed]
11. Rai, M.; Yadav, A. Plants as potential synthesiser of precious metal nanoparticles: Progress and prospects. *IET Nanobiotechnol.* **2013**, *7*, 117–124. [CrossRef] [PubMed]

12. Kulkarni, N.; Muddapur, U. Biosynthesis of Metal Nanoparticles: A Review. *J. Nanotechnol.* **2014**, *2014*, 510246. [CrossRef]
13. Karman, S.B.; Diah, S.Z.M.; Gebeshuber, I.C. Raw Materials Synthesis from Heavy Metal Industry Effluents with Bioremediation and Phytomining: A Biomimetic Resource Management Approach. *Adv. Mater. Sci. Eng.* **2015**, *2015*, 185071. [CrossRef]

Disclaimer/Publisher's Note: The statements, opinions and data contained in all publications are solely those of the individual author(s) and contributor(s) and not of MDPI and/or the editor(s). MDPI and/or the editor(s) disclaim responsibility for any injury to people or property resulting from any ideas, methods, instructions or products referred to in the content.